



# Parameter estimation of river incision models of soft sedimentary rocks – a case study on the Kamikita Coastal Plain, northeast Japan

Shizuka Takai<sup>1</sup>, Tomoji Sanga<sup>2</sup>, Taro Shimada<sup>1</sup>, and Seiji Takeda<sup>1</sup>

<sup>1</sup>Nuclear Safety Research Center, Japan Atomic Energy Agency, Ibaraki, 319-1195, Japan

<sup>2</sup>SNG Consultant, Saitama, 335-0013, Japan

**Correspondence:** Shizuka Takai (takai.shizuka@jaea.go.jp)

Received: 19 January 2026 – Discussion started: 4 February 2026

Revised: 24 April 2026 – Accepted: 11 May 2026 – Published: 2 June 2026

**Abstract.** Understanding river incision model is crucial for predicting long-term landscape evolution. For the bedrock channel incision model (detachment-limited (DL) model: erosion rate  $E = K A^m S^n$  where  $A$  is drainage area,  $S$  is channel gradient), parameters ( $K$ ,  $m$ , and  $n$ ) can be estimated via slope-area analysis if  $E$  is known. Using  $^{10}\text{Be}$  denudation rate, previous studies globally compiled the parameter values for variable lithology. However, limited data availability for soft sedimentary rock restricts the applicability of global compilation. In addition, measuring the  $^{10}\text{Be}$  concentration in sedimentary rock is challenging in humid and tectonically active regions. To address this, slope-area analysis was conducted in the Kamikita Coastal Plain, Japan, where lithology (Miocene to Pleistocene sedimentary rocks) and uplift rate ( $\sim 0.2 \text{ mm yr}^{-1}$  for the past 300 ka) are assumed to be uniform. River incision rates were derived approximately from widely distributed marine terraces (MIS 5e–11). For six target rivers, DL-like behaviour was confirmed in the limited areas located upstream of the alluvium distribution. The reference concavity  $m/n$  was  $0.44 \pm 0.10$ , typical for steady-state channels. Across the  $m/n$  range of 0.4–0.6, the exponent  $n$  consistently exhibited nonlinearity ranging between 1.14 to 1.34, which is consistent with the previous global compilations. This observed nonlinearity likely reflects transient landscape responses to past sea-level changes, which generated slope-break knickpoints at similar elevations. Finally, the estimated erosion coefficient  $K$  ( $10^{-5}$ – $10^{-6}$ ) agreed with the global relationship with unconfined compressive strength  $q_u$  ( $K \propto 1/q_u^2$ ), supporting the significant influences of bedrock lithology on  $K$ .

## 1 Introduction

Prediction of long-term landscape evolution is indispensable for social planning and infrastructure management, such as radioactive waste repositories, mine waste deposits, and landfills. In several fields, long-term assessments spanning  $10^4$ – $10^5$  years are required to confirm geological stability; for instance, carbon dioxide capture and storage ( $\sim 10\,000$  years: IPCC, 2005; Alcalde et al., 2018) and radioactive waste disposal (100 000 years for intermediate-level waste: e.g., SSM, 2008; NRA, 2021). To ensure reliable risk assessment for these facilities, including the evaluation of future erosion depths and their effects on groundwater flow systems, past landscape evolution since the Late Quaternary

(i.e., the last glacial–interglacial cycle since 125 ka) must be elucidated. Among various landscape processes, river incision is one of the main drivers of landscape evolution and can cause considerable vertical erosion (e.g., Whipple, 2004). Therefore, a quantitative understanding of river incision models and their parameters is essential for robust long-term projections of erosion depth.

River incision models are broadly classified into two types: the detachment-limited (DL) model and the transport-limited (TL) model. The DL model assumes that all particles eroded by the river are immediately removed from the system. The long-term river incision rate  $E$  [ $\text{L T}^{-1}$ ] is controlled by shear stress or stream power per unit width on the

bed (e.g., Howard and Kerby, 1983; Howard, 1994; Whipple and Tucker, 1999). Under idealized circumstances,  $E$  is described as a simple function of both channel slope  $S$  [–] and upstream drainage area  $A$  [ $L^2$ ] as follows (stream power incision model):

$$E = K A^m S^n, \quad (1)$$

where  $m$  and  $n$  are positive constants ( $\theta = m/n$  is the concavity index).  $K$  [ $L^{1-2m} T^{-1}$ ] is the erosion coefficient reflecting the combined influences of bed erodibility, climate and downstream changes in channel hydraulic geometry. On the other hand, the TL model assumes that sediment flux  $Q_s$  [ $L^2 T^{-1}$ ] transported by the river is limited by its transport capacity (Henderson, 1966; Hergarten, 2020):

$$Q_s \propto A^{m+1} S^n. \quad (2)$$

The values of  $S$  and  $A$  can be easily calculated based on digital elevation model (DEM). Therefore, if  $E$  is known and the environment (i.e., tectonics, lithology, and climate) is uniform, the river incision parameters ( $m$ ,  $n$ , and  $K$ ) can be estimated from the field data and the DL model (e.g., Kirby and Whipple, 2012; Lague, 2014). When using data from rivers with different drainage areas, a reference concavity  $\theta_{\text{ref}}$ , generally the regional mean of observed  $\theta$ , is used for comparison purposes.

In recent decades, river incision parameters have been estimated in various regions (e.g., Kirby and Whipple, 2012; Lague, 2014; Harel et al. 2016; Hilley et al., 2019; Adams et al., 2020; Desormeaux et al., 2022; Hu et al., 2023; Marder and Gallen, 2023; Ott et al., 2023) and global compilations have been conducted using this data. For example, Lague (2014) estimated the parameters for 10 basins globally distributed and found that  $n \sim 2$  (ranging from 1 to 4) using  $\theta_{\text{ref}} = 0.45$ . Harel et al. (2016) compiled the parameter values at 59 study areas of various lithology, climatic, and tectonic settings. Using  $\theta_{\text{ref}} = 0.5$ , a mean ( $\pm 1\sigma$ )  $n$  of 2.7 ( $\pm 2.9$ ) was suggested. Moreover, Haag and Schoenbohm (2025) indicated that the global compiled  $K$  in Harel et al. (2016) is inversely proportional to the square of unconfined compressive strength  $q_u$ :  $K \propto 1/q_u^2$ .

However, there are two problems with the above studies. First, previous research ( $q_u \geq 15$  MPa: Haag and Schoenbohm, 2025) lacks data of soft sedimentary rocks. This is especially important for tectonically active regions like Japan where over 50 % of the surface geology consists of Paleogene and Neogene sedimentary rocks (NUMO, 2021). Nevertheless, river incision parameters and its relationship with  $q_u$  have not been discussed for soft sedimentary rocks with  $q_u = 1$ –10 MPa. Second, previous parameter estimations have primarily relied on basin average denudation rates derived from cosmogenic radionuclides (CRN), such as beryllium-10 ( $^{10}\text{Be}$ ) in quartz grains from river sediments. However, it is difficult to measure the  $^{10}\text{Be}$  concentration for sedimentary rocks in humid and tectonically active regions like Japan due to the lack of quartz and the diversity

of topographic deformation and sedimentation-erosion processes (AIST, 2016). In such regions, the  $^{10}\text{Be}$  measurement is appropriate for quartz-rich rocks, such as granite (e.g., Takahashi et al., 2023). Furthermore, CRN-derived denudation rates typically reflect relatively short-term durations, which are roughly inversely proportional to the incision rate (Lal, 1991). Therefore, CRN-derived denudation rates reflect average timescales of  $10^5$  years in active regions with erosion rates of several  $\text{mm kyr}^{-1}$ , but only  $10^2$ – $10^3$  years in tectonically active regions with several  $\text{m kyr}^{-1}$  erosion (von Blanckenburg, 2006). Another conventional approach is to assume a topographic steady state (e.g., Snyder et al., 2000; Kirby and Whipple, 2001; Duvall et al., 2004). However, many environments have not yet attained a steady state (Bishop et al., 2005; Campforts and Govers, 2015; Vanacker et al., 2015; Armitage et al., 2018). Especially in coastal areas, the landscape has been drastically changed due to periodic sea-level change. Thus, as Lague (2014) noted, deriving locally measured incision rates from dated terraces remains one of the least potentially biased methods for quantifying long-term incision. However, only a few studies (e.g., Lague, 2014) address this issue by using reach incision rates based on strath terraces.

To address these issues, we performed slope-area analysis in the Kamikita Coastal Plain, Japan, where bedrock lithology (sedimentary rocks of Miocene to Pleistocene) and uplift rate are assumed to be uniform. Parameter values were estimated based on river incision rates approximately derived from marine terraces (Marine Isotope Stages (MIS) 5e, 7, 9, and 11) widely distributed in the area. First, we estimated the validity range of the DL model and  $\theta$  for six target rivers. Then, we estimated the river incision parameters using the erosion rates approximately evaluated from the marine terraces. Finally, we confirmed the validity of the estimated parameter values by comparing them with those from previous global compilations.

## 2 Study area

The Kamikita Plain in northeast Japan is a vast coastal plain approximately  $30 \times 50 \text{ km}^2$ , located along the coastline of Pacific Ocean (Fig. 1a). In this region, Middle and Late Pleistocene marine terraces are widely preserved at multiple levels (Fig. 2a): the Takadate terrace (MIS 5e), the Tengu-dai terrace (MIS 7), the Shichihyaku terrace (MIS 9), and the higher terrace (MIS 11) (AIST, 2016). The chronology has been estimated using various techniques: sediment rate chronology (Miyouchi, 1985; Koike and Machida, 2001), optically stimulated luminescence (AIST, 2015, 2016), and tephra and phytolith stratigraphy (Kuwabara, 2004, 2007, 2009; Matsu'ura et al., 2019). Based on these previous studies, Matsu'ura et al. (2019) concluded that the uplift rate of the Kamikita Plain (around Lake Ogawara) has been constant at approximately  $0.2 \text{ mm yr}^{-1}$  over the last 300 ka.

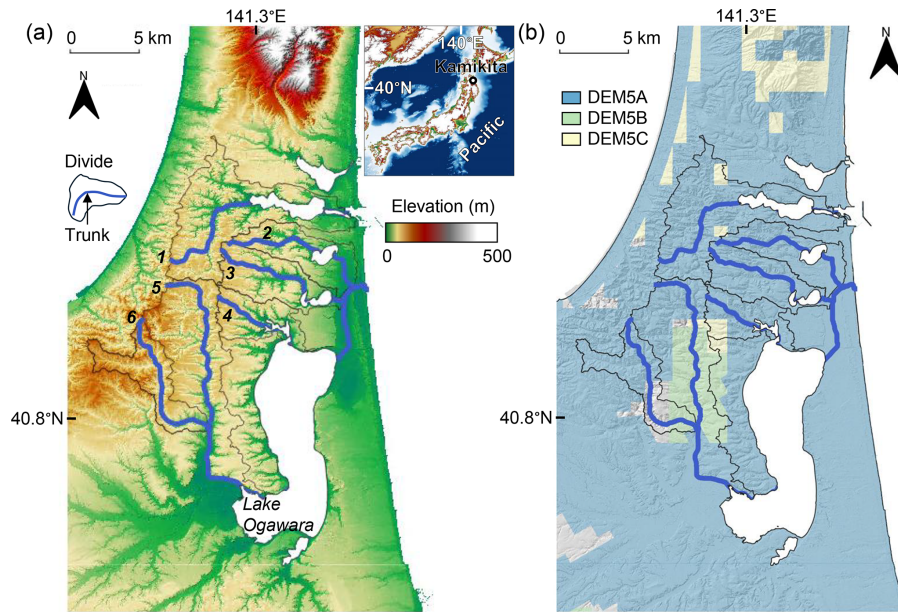


**Figure 1.** (a) Topography and (b) provided area of 5 m DEM by Geospatial Information Authority of Japan. For area where 5 m DEM is not provided, 10 m DEM was used.

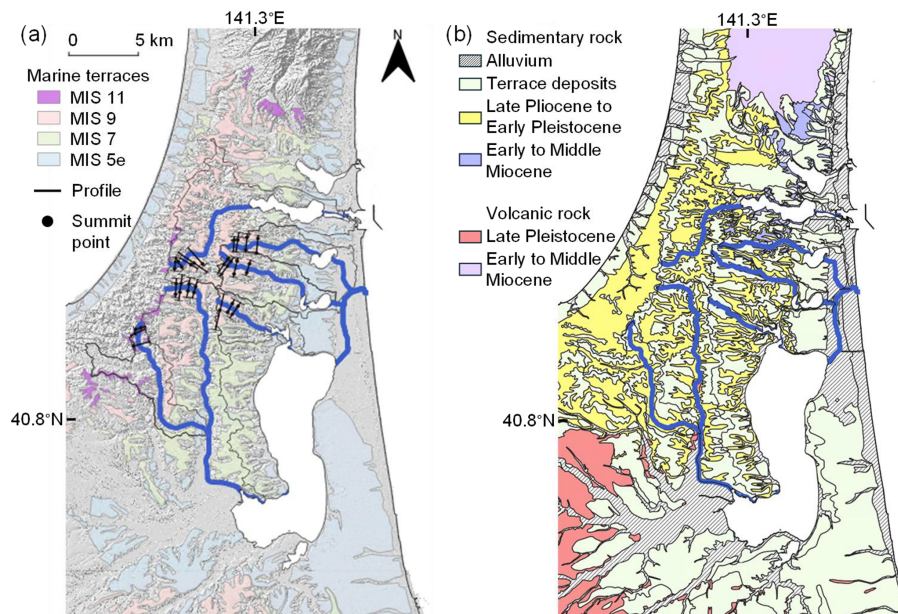


**Figure 2.** (a) Marine terraces and (b) geology of the study area. Marine terraces are based on Koike and Machida (2001). Geological map is based on the 1 : 200 000 scale geologic map (AIST, 2025). The summit levels extracted from profiles of the marine terrace surfaces were used for erosion rate estimates. Geological units are based on Kudo (2020).

Geological units of the Kamikita Plain are summarised by Kudo et al. (2020) (Fig. 2b). Bedrock was formed in the early to middle Miocene: the Takahoko Formation, sedimentary rock (16.6–13.1 Ma), which is mainly composed of pumice tuff, sandstone, and mudstone (Inohara et al., 2008), and the Tomari Formation, volcanic rock (16.6–15 Ma), characterized by basaltic to andesitic lavas and pyroclastic rocks

(Kudo et al., 2020). Sedimentary rock units of late Pliocene to early Pleistocene, the Hamada Formation and the Katchi Formation, which primarily consist of sandstone and siltstone (Nemoto and Ujiie, 2009), overlay the bedrock. These sedimentary rocks are covered by terrace deposits of middle to late Pleistocene and alluvium. The mean annual rainfall in this region is around 1300 mm (JMA, 2026).

**Table 1.** Target rivers. Drainage area and length include coastal lagoons.

No.	River	Drainage Area (km <sup>2</sup> )	Length (km)	Valley-head elevation (m)
1	Togusari River	55.9	18.7	64.8
2	Ishiwatari River	23.0	12.9	67.9
3	Hiranuma River	24.6	12.7	74.7
4	Uchinuma River	16.2	7.1	63.7
5	Doba River	74.4	22.2	73.5
6	Gandosawa River	74.4	20.2	93.5

The Continental Divide is located in the western part of the study area. The valleys are deep on the west side of the divide and shallow on the east side. The rivers on the east side dissect the marine terraces and flow into the Pacific Ocean. Downstream the rivers, coastal lagoons such as Lake Ogawara are located, which were formed by sea-level fall during the Last Glacial Maximum and by subsequent development of sandbanks during the post-glacial period. In this study, we examined six streams flowing into the Pacific Ocean (1: the Togusari River, 2: the Ishiwatari River, 3: the Hiranuma River, 4: the Uchinuma River, 5: the Doba River, 6: the Gandosawa River) (Table 1), whose lithologic (sedimentary rock of Miocene to Pleistocene) and tectonic conditions (uplift rate  $\sim 0.2 \text{ mm yr}^{-1}$ ) can be assumed to be uniform. Note that the rivers No. 2–6 are tributaries of the Takase River, which has a drainage area of  $867 \text{ km}^2$  (MLIT, 2006) and flows from the Hakkoda Mountains located west of the study area. Volcanic rocks are distributed throughout the region and the tectonics differ from that of the Kamikita Plain; therefore, the Takase River was excluded from the scope of this study.

### 3 Methods

As previous research has shown (e.g., Whipple and Tucker, 2002; Whipple, 2004), most bedrock channels are mixed bedrock-alluvial channels partially covered by alluvium. In this case, the river profile consists of colluvial, bedrock, and alluvial sections (Fig. 3a). Empirical evidence suggests that many river profiles across different geological settings follow a power-law relationship between  $S$  and  $A$ , known as Flint's law (Hack, 1957; Morisawa, 1962; Flint, 1974):

$$S = k_s A^{-\theta}, \quad (3)$$

where  $k_s$  [ $\text{L}^{2\theta}$ ] is the steepness index. The detachment-limited stream power incision model (Eq. 1) also predicts a similar slope-area scaling. Under the assumptions that  $K$  is constant (e.g., spatially uniform lithology and climate) and  $E$  has been measured (e.g., Hilley et al., 2019), the parameters in Eq. (1) can be inferred from  $k_s$  ( $= (E/K)^{(1/n)}$ ) and  $\theta$

( $= m/n$ ) estimated using Eq. (3), without measuring stream power directly.

Equation (3) implies that in detachment-limited reaches, the log-transformed slope-area plot can be fitted with a linear regression (Fig. 3b). Since channel transitions from bedrock to alluvial (i.e., DL to TL) or colluvial processes typically cause changes in channel slope (e.g., Whipple and Tucker, 1999, 2002; Stock et al., 2005), sections can be identified using the slope-area plot (Wang et al., 2017). Above a critical drainage area ( $A_c$ ), colluvial processes, such as debris flows and land sliding, are dominant (Wobus et al., 2006). Below  $A_c$ , the fluvial processes dominate. Both the bedrock and alluvial sections exhibit a descending gradient with increasing drainage areas (Whipple and Tucker, 2002). However, the transition to alluviated conditions causes a sudden reduction in channel gradient (Wobus et al., 2006).

Channels may contain knickpoints, which can be classified into two categories: vertical-step knickpoints and slope-break knickpoints (Fig. 3c). Vertical-step knickpoints correspond to sudden changes in elevation, such as waterfalls, and can be identified as spikes on the slope-area plot. These knickpoints are generally caused by channel-scale heterogeneities such as bounding faults (e.g., Kirby and Whipple, 2012; Liu et al., 2020).

Herein, we focused on slope-break knickpoints because they represent channel response to regional-scale perturbations, such as lithologic heterogeneity and sea-level fall (e.g., Haviv et al., 2010; Kirby and Whipple, 2012; Boulton, 2020). Unlike vertical-step knickpoints, these features mark a fundamental shift in the channel gradient, leading to abrupt changes in flow conditions. By identifying these slope-break knickpoints, we can evaluate how regional-scale factors influence river incision parameters.

This study estimated river incision parameters in three consecutive steps. First, sections exhibiting DL-like behaviours were identified from slope-area plots. Their validity was confirmed by comparing them with the alluvium distribution. We used a 5 m gridded digital elevation model (DEM), which is provided by the Geospatial Information Authority of Japan (Fig. 1b). Three types of 5 m DEM collected by different methods were combined: DEM5A (airborne LiDAR measurements), DEM5B and DEM5C (photogrammetry). There is also a 10 m DEM covering the entire country, which is created by interpolating topographic contour map with 10 m intervals. However, such a DEM can cause problems, such as artificial knickpoints due to interpolation errors or short-circuit meander bends in a river profile (Wobus et al., 2006). Therefore, we used the higher-resolution 5 m DEM. In areas where 5 m DEM is not available, such as the southeastern part of the Doba River and the middle of the Gandosawa River, 10 m DEM was bilinearly resampled to 5 m point spacing. Using the ArchHydrology toolbox (Tarboton et al., 1991), streams were extracted by applying a D8 flow routing algorithm and the trunk was defined from the Horton-Strahler number. To circumvent noise, previous research (Wobus et

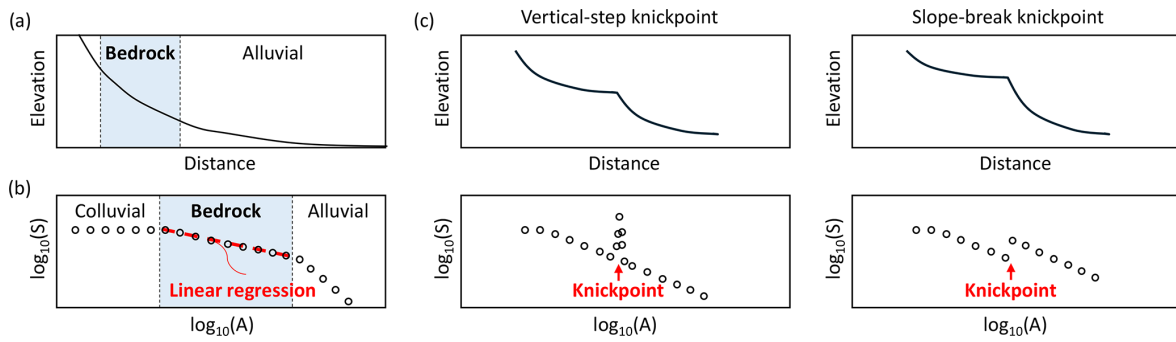


**Figure 3.** Schematic of (a) river profile, (b) slope-area plot, and (c) knickpoints (revised from Snyder et al., 2000, and Whipple et al., 2013).

al., 2006; Whipple et al., 2007) has indicated that DEM-derived river profiles require the implication of some smoothing algorithms, such as a moving-window average. Furthermore, calculating the averaged channel slopes at a certain elevation interval or logarithmic bins of drainage area (log-bin averaging) was suggested (e.g., Snyder et al., 2000; Wobus et al., 2006). In previous studies utilizing the USGS 10 m DEM (root mean square error = 2.44 m; Gesch, 2007), Wobus et al. (2006) used moving-window sizes of 200 or 400 m, whereas Whipple et al. (2007) suggested an optimal window size of 250 m. The DEM datasets used herein possess a maximum measurement error (standard deviation) of 5 m, with specific accuracies ranging from 0.3 m (DEM5A), 0.7 m (DEM5B), 1.4 m (DEM5C), to 5 m (10 m DEM) (GIA, 2026). To ensure analytical consistency across the entire catchment and account for the largest measurement error, we smoothed elevation data using a 500 m moving window and calculated averaged slopes on 5 m contours and log-bin averaged slopes. We verified that no artificial knickpoints were generated at DEM tile boundaries.

In the second step, we calculated the channel concavity index from the integral approach within the detachment-limited reaches (Perron and Royden, 2013):

$$\chi = \int_{x_b}^x \left( \frac{A_0}{A(x)} \right)^\theta dx, \quad (4)$$

$$z(x) = z(x_b) + \left( \frac{E}{KA_0^m} \right)^{1/n} \chi = z(x_b) + \left( \frac{k_s}{A_0^\theta} \right) \chi, \quad (5)$$

where  $x$  [L] is the horizontal upstream distance from an outlet;  $x_b$  [L] is the distance at the outlet (in this study,  $x_b = 0$ ); and  $z$  [L] is elevation. The validity of the bedrock sections identified by slope-area plots is confirmed again by the linearity of  $\chi$  plot. As shown in Eqs. (3) and (5), local  $k_{sn}$  values and their channel-averaged values can be calculated either from (1) the slope-area approach (e.g., Wobus et al., 2006; Scherler et al., 2014) or (2) the slope of  $\chi$  plots (hereafter  $k_{sn-\chi}$ : e.g., Perron and Royden, 2013; Gailleton et al., 2019). The slope-area approach preserves local signals associated with knickpoints, whereas  $k_{sn-\chi}$  is comparatively

smoother and less sensitive to noise (Gailleton et al., 2019). Previous studies have compared these two approaches (e.g., Scherler et al., 2014; Neely et al., 2017) and demonstrated that the choice of method should depend on the context and objective of a study. In this study, we primarily used local  $k_{sn}$  ( $= SA^{\theta_{ref}}$ ) and its channel-averaged values derived from the slope-area approach (e.g., Takahashi et al., 2022). This is because our objectives include investigation of the transient steepening and lithological signals associated with slope-break knickpoints, which may be partially smoothed in  $k_{sn-\chi}$  despite its lower sensitivity to noise. For channel-averaged  $k_{sn}$ ,  $k_{sn-\chi}$  was additionally calculated to evaluate the robustness of the results.

Using a reference basin area of  $A_0 = 1 \text{ m}^2$ , the concavity index ( $\theta$ ) and knickpoint locations were estimated using a statistical segment-fitting algorithm (Mudd et al., 2014). In this algorithm, the optimal  $\theta$  is evaluated in  $\chi$  space by minimizing the corrected Akaike Information Criterion (AICc) across all possible contiguous channel segments.

$$\text{AICc} = \text{AIC} + \frac{2k(k+1)}{N-k-1}, \quad \text{AIC} = 2k + \frac{\text{RSS}}{\sigma_z^2} \quad (6)$$

where  $N$  is the number of channel nodes,  $s$  is the number of segments ( $k = 2s$ ), RSS is the residual sum of squares between data points and regression lines, and  $\sigma_z$  is the standard deviation of elevation measurements, including geomorphic noise. In this study, we used DEM5A (standard deviation: 0.3 m) in detachment-limited reaches, and  $\sigma_z$  was conservatively set to 0.6 m. A bootstrapping method was employed with 1000 independent trials to evaluate the robustness of the results. In this method, channel nodes were randomly skipped using a uniform distribution ranging from 0 to  $2 \times n_{sk}$ . Following Gailleton et al. (2019),  $n_{sk}$  was set to 1.  $\theta_{ref}$  was determined using a collinearity test that minimized the sum of AICc values across all analyzed rivers. Because  $\chi$  profiles were segmented into channel reaches of unequal length, channel-averaged  $k_{sn-\chi}$  was calculated as the stream-length-weighted mean of segment slopes to avoid overrepresentation of short reaches. Knickpoints were defined as boundaries between adjacent segments. Knickpoint type was classified using the slope ratio of regression lines ( $S_{ratio}$ ) and

elevation difference ( $Z_{\text{jump}}$ ) across these boundaries: large  $Z_{\text{jump}}$  with a minimal change in  $S_{\text{ratio}}$  indicates a vertical-step knickpoint, whereas a significant change in  $S_{\text{ratio}}$  with negligible  $Z_{\text{jump}}$  indicates a slope-break knickpoint. In accordance with Gailleton et al. (2019), knickpoints were extracted using the optimal  $\theta$  specific to each river. To remove minor knickpoints, we applied thresholds of  $Z_{\text{jump}} = 5.0$  m and  $S_{\text{ratio}} = 0.2$ . These values are broadly consistent with those used in previous studies: Neely et al. (2017) applied a minimum knickzone height of 5 m for 10 m DEM, and Gailleton et al. (2019) used a threshold of  $|\Delta k_{sn}|$  (the difference in slope of regression lines) = 0.8 for  $k_{sn}$  values ranging from 0.5 to 5.0.

In the third step, the values of  $n$  and  $K$  were estimated. Within the detachment-limited reaches, the relationship between  $E$  and  $k_{sn}$  is expressed as:

$$E = K k_{sn}^n. \quad (7)$$

Taking the natural logarithm of Eq. (7) allows  $n$  and  $K$  to be estimated via the regression analysis of  $E$  and  $k_{sn}$  (e.g., Leonard et al., 2023):

$$\ln(E) = n \ln(k_{sn}) + \ln(K), \quad (8)$$

where  $n$  and  $\ln(K)$  represent the slope of the regression line and the intercept, respectively. River terraces are not identified in the study area (Koike and Machida, 2001). Since the target rivers incising marine terraces have smooth and concave-up profiles, long-term incision rate  $E$  was approximately calculated based on the height of marine terraces:

$$E = (z_t - z_r - d) / T_t, \quad (9)$$

where  $z_t$  [L] is the summit level of the marine terrace;  $z_r$  [L] is the present river profile;  $d$  [L] is the thickness of tephra and loess; and  $T_t$  [T] is the formation age of the river. The summit level of the marine terrace was reconstructed by interpolating the highest elevations from multiple topographic profiles extracted from preserved marine terrace surfaces (Fig. 2a; see Figs. S1–S6 in the Supplement for detailed maps and profiles). Where summit levels were comparable on both banks of the river, their average value was used.  $T_t$  was approximated as the terrace age where valley head is located.

To ensure spatial consistency,  $E$  and  $k_{sn}$  were compared at equal intervals of 200 m along the river channels, following the approach for parameter estimation using strath terraces by Lague (2014). To account for uncertainties in  $E$  (Eq. 9), a Monte Carlo simulation with 100 000 iterations was performed based on the inherent probability distribution of all input parameters (Table 2). Elevation uncertainty was modeled as a Gaussian distribution based on DEM precision (0.3 m for DEM5A) in the detachment-limited reaches. The uncertainties in terrace age ( $T_t$ ) and tephra thickness ( $d$ ) were represented using uniform distributions derived from field observations.

$T_t$  values were adapted from those reported by Matsu'ura et al. (2019) for the Kamikita Coastal Plain: 398 to 410 ka (MIS 11), 318 to 324 ka (MIS 9c), 230 to 235 ka (MIS 7e), 212 to 220 ka (MIS 7c), and 116 to 132 ka (MIS 5e). Furthermore,  $d$  values were derived from observed data of tephra layers and loam (tephric loess) in the study area. The main tephra layers are as follows (Kudo, 2023): Hakkoda second-stage (Hkd2: 0.19–0.29 Ma) and White Pumice (WP: 210 ka) erupted from the Hakkoda Volcano; Orange Pumice (OrP: 166 ka) and Towada-Ofudo (To-Of: 36 ka) erupted from the Towada Volcano; and Toya (106 ka) erupted from the Toya Volcano. Based on outcrop observations at seven locations, AIST (2015, 2016) has identified the tephra and loam thickness as 11.4 m (sampled at Onadesawa) and 10.5 m at Kanaya for MIS 11; 14 m at Shichihyaku and 7 m at Kamiyoshita for MIS 9; 6 m at Hotozawa for MIS 7; 2 m or 4 m at Neinuma for MIS 5e (the outcrop locations: Fig. S7). For the MIS 5e marine terraces, Koike and Machida (2001) indicated that the thickness of cover deposit layers is 2 m at four points to 3 m at one point. Note that Kudo (2023) provides an approximate estimate of the spatial distribution of tephra thickness for the Towada Volcano. However, this information is not provided for other volcanoes. Accordingly, a uniform thickness was assigned to each terrace stage (Table 2). This Monte Carlo approach enables the evaluation of the parameter reliability by accounting for uncertainties in summit level, riverbed elevation, tephra thickness, and marine terrace age.

## 4 Results

### 4.1 Channel profiles

Longitudinal river profiles, slope-area plots, and  $\chi$  plots for six rivers are shown in Fig. 4.  $A_{cr}$  is confirmed at  $\sim 0.1$  km<sup>2</sup> for all rivers, which is consistent with earlier studies (e.g., Montgomery and Foufoula-Georgiou, 1993; Stock and Dietrich, 2003; Wobus et al., 2006). In the slope-area plots (Fig. 4b), all rivers exhibit an approximately linear descending gradient with increasing drainage areas. The gradients suddenly reduce around  $A = 1$ –10 km<sup>2</sup> upstream of the alluvium distribution. This is consistent with previous research on mixed bedrock and alluvial channels (Snyder et al., 2000; Wobus et al., 2006; Wang et al., 2017), reflecting a transition to alluviated conditions due to the sea level rise during the Holocene. Therefore, the studied rivers are considered to be mixed bedrock and alluvial channels, and the sudden decrease in the channel gradient corresponds to the transition from erosive bedrock channels (DL) to depositional alluvial channels (TL).

The  $\theta$  values estimated for detachment-limited reaches are summarised in Table 3 and Fig. 5. The optimal  $\theta$  values for each river range from 0.18 to 0.59 (Fig. S8 shows the AICc values). Meanwhile,  $\theta_{\text{ref}}$  was estimated to be  $0.44 \pm 0.10$  (standard deviation) using the collinearity test (Fig. 5b), which lies within the general range of steady-state channels

**Table 2.** Probability distribution used for uncertainty analysis of erosion rate.

Parameter	Assigned distribution	Values
$z_t$ Summit level (m)	Gaussian	Mean: reconstructed summit level $\sigma$ : standard deviation within 200 m interval
$z_r$ Riverbed (m)	Gaussian	Mean: elevation extracted from DEM $\sigma$ : 0.3 m (standard error of DEM5A)
$d$ Tephra thickness (m)	Uniform	MIS 9: [7.0, 14.0], MIS 11: [10.5, 11.4]
$T_t$ Marine terrace age (ka)	Uniform	MIS 9c: [318, 324], MIS 11: [398, 410]

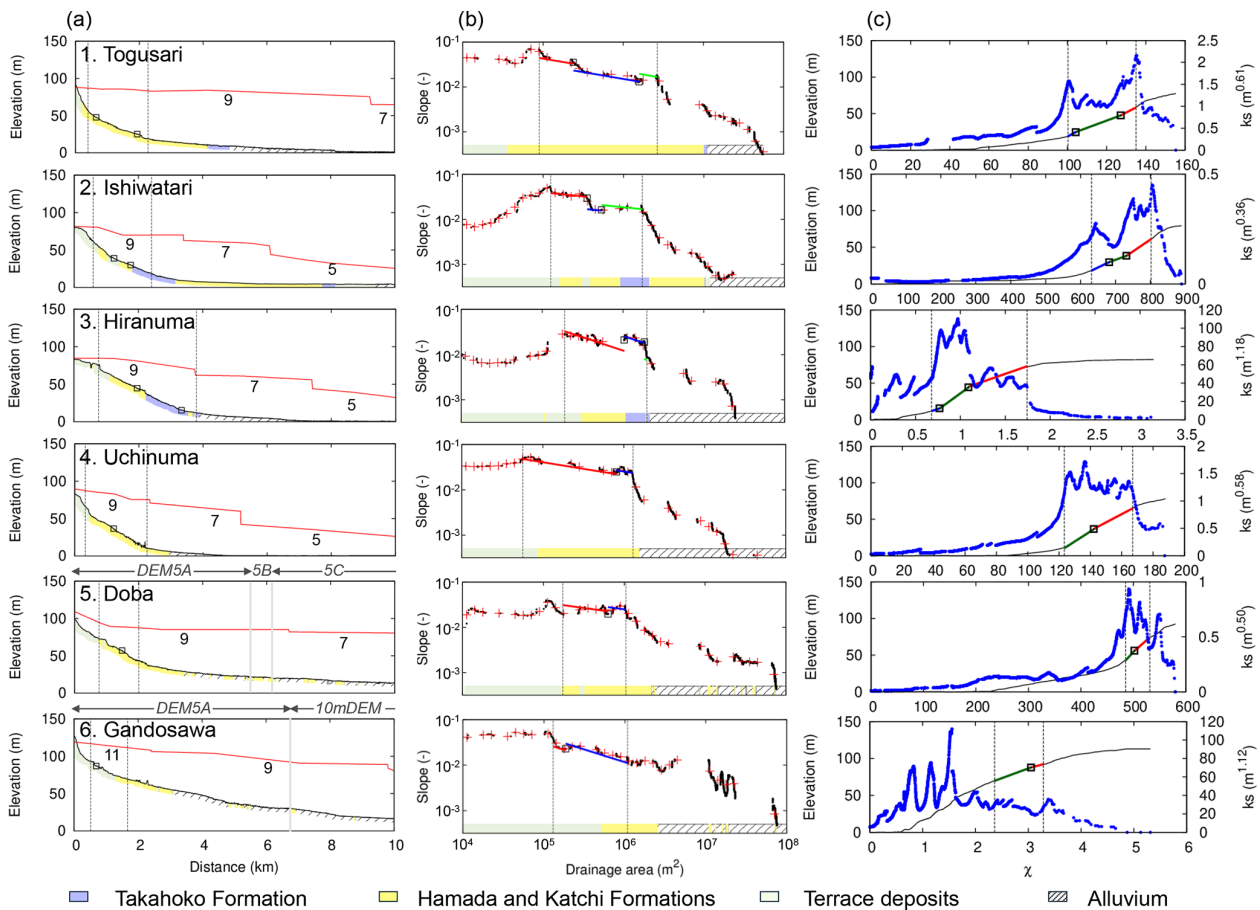


**Figure 4.** Stream profile analysis of the study area. **(a)** Longitudinal profile (black line) and the elevation of marine terraces (red line) with Marine Isotope Stages. Squares denote knickpoints. Gray lines for rivers No. 5 and 6 indicate the boundaries of DEMs other than DEM5A (LiDAR 5 m DEM). **(b)** Slope-area plot. Average channel slopes are calculated on 5 m contours (black point) and by the log-bin averaging method (red mark). **(c)**  $\chi$  plot (black line) with  $k_s$  (blue point) based on the concavity of each river. In all graphs, dashed lines and color bold lines (red, blue, and green) correspond to the bedrock section and its regression line.

( $\theta = 0.35\text{--}0.6$ : Kirby and Whipple, 2012) and closely aligns with the typical reference concavity of 0.45 (e.g., Wobus et al., 2006). Snyder et al. (2003) indicates that even considering sea-level changes, a quasi-steady-state condition has been achieved in the upper parts of the channel. Therefore, although the target rivers tend to fluctuate from their mouths

to their divides reflecting sea-level change, it can be assumed that they have approached the quasi-steady state in the upstream section. However, as  $\theta_{ref}$  can impact the estimation of river incision parameters, we evaluated  $k_{sn}$  using  $\theta_{ref}$  values of 0.4, 0.5, and 0.6 to ensure robustness.

**Table 3.** Formation ages and concavity indices (with standard deviation).

No.	1	2	3	4	5	6
Formation Age	MIS 9	MIS 9	MIS 9	MIS 9	MIS 9	MIS 11
$\theta$	$0.30 \pm 0.06$	$0.18 \pm 0.04$	$0.59 \pm 0.04$	$0.29 \pm 0.05$	$0.25 \pm 0.15$	$0.56 \pm 0.03$

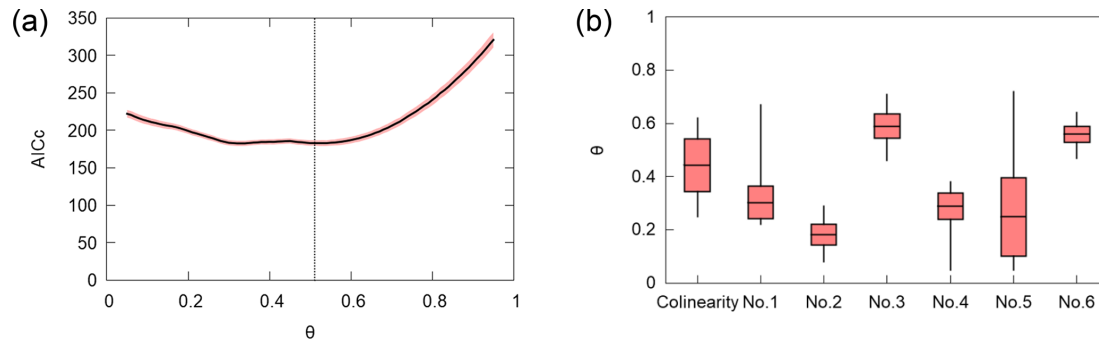
**Figure 5.** (a) AICc values for the regional collinearity test and (b) the distribution of optimal  $\theta$  for regional and individual river basins. In panel (a), the solid line and shaded red area indicate the mean and  $\pm 1\sigma$  (standard deviation) interval for 1000 bootstrap trials. In panel (b), the whiskers indicate the range between minimum and maximum values, while the boxes represent the mean and  $\pm 1\sigma$  interval.

Table 4 and Fig. 6 show the extracted knickpoints and their locations on the map (Fig. 4c). All knickpoints are classified as slope-break knickpoints and do not correspond to the boundaries between different DEM datasets. Except for the second knickpoint of river No. 2, the knickpoints are not located near lithological boundaries. Instead, they are distributed at similar elevations (around E.L. 25 and 50 m). This suggests that they can be base-level-fall related upstream-migrating knickpoints. In the Sanriku Coast, approximately 50 km south of the study area, Ogami (2015) identified upstream-migrating knickpoints in multiple rivers which were formed during the sea-level highstands during MIS 5e, 7, 9, and 11. The knickpoints in the study area may have been formed for the same reason. Note that in river No. 6, which formed earlier than the other rivers (MIS11), a knickpoint is observed at a higher elevation of 88 m. This knickpoint could have been formed during a preceding sea-level cycle.

The second knickpoint of river No. 2 is located near the boundary between the Hamada and Katchi Formations and the Takahoko Formation (Fig. 4a). As discussed in Sect. 5.2, the Takahoko Formation exhibits higher  $N$ -values (80–137) compared with the Hamada and Katchi Formations (50–63). This contrast in rock hardness likely contributed to the formation of this lithological knickpoint. The same boundary is also located near the first knickpoint of river No. 3; however, because its elevation is close to 50 m, this knickpoint might be affected by both the lithological difference and sea-level changes.

**Table 4.** Extracted knickpoints.

River No.	Knickpoint	Elevation (m)	$Z_{\text{jump}}$ (m)	$S_{\text{ratio}}$ (–)
1	Slope-break	47.8	–0.05	0.71
	Slope-break	24.8	0.05	1.49
2	Slope-break	38.8	–0.13	0.53
	Slope-break*	29.8	0.02	1.34
3	Slope-break	45.3	–0.71	2.10
	Slope-break	15.9	–0.04	0.44
4	Slope-break	36.7	–0.50	1.22
5	Slope-break	56.4	0.11	1.24
6	Slope-break	88.1	0.01	1.41

\* This knickpoint is located approximately 50 m upstream from the lithological boundary (Hamada/Katchi and Takahoko Formations) along the river channel.

#### 4.2 River incision parameters

$E$  and  $k_{sn}$  were compared at 200 m intervals along the river channels (Fig. 7a–c). A positive correlation between  $E$  and  $k_{sn}$  was observed across all  $\theta_{\text{ref}}$  values. The correlation coefficient ( $R$ ) increased with increasing  $\theta_{\text{ref}}$ , ranging from 0.37 to 0.59. Across the range of  $\theta_{\text{ref}} = 0.4$ –0.6, the estimated  $n$  values consistently indicated a nonlinear relationship ( $n > 1$ ) and fell within a narrow range from 1.14 to 1.34. In contrast, the estimated  $K$  varied over a considerably wider range from  $4.2 \times 10^{-7}$  to  $1.3 \times 10^{-5}$ . The 90% confidence intervals for these parameters were  $n = [0.94, 1.28]$ ,  $[1.15, 1.46]$ , and

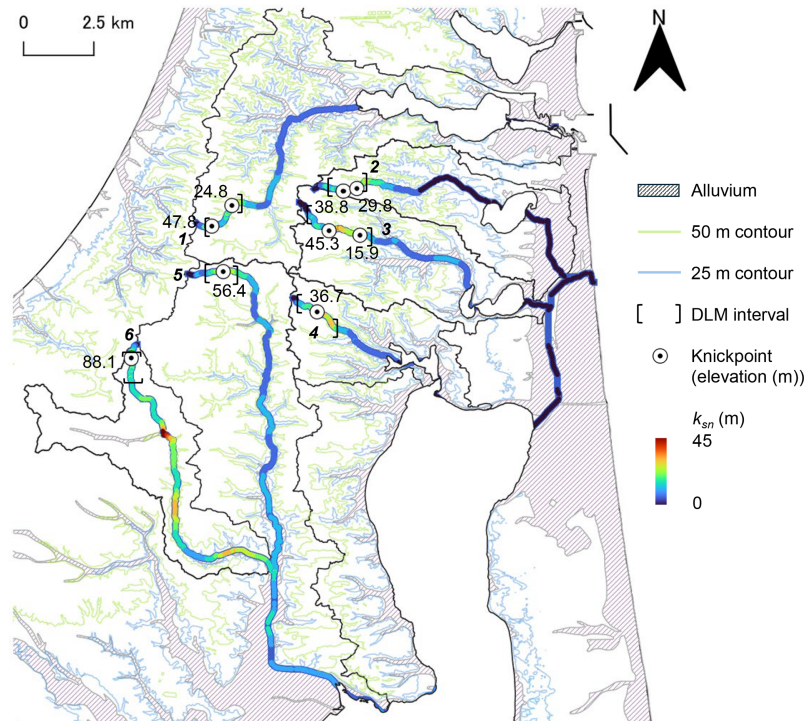


**Figure 6.** Knickpoints (points with elevation (m)) and 25 and 50 m contours (blue and green lines) within the detachment-limited reaches. Color along the rivers demonstrates  $k_{sn}$  ( $\theta_{ref} = 0.5$ ).

[1.10, 1.36], and  $K = [1.0 \times 10^{-6}, 2.9 \times 10^{-6}]$ ,  $[1.1 \times 10^{-6}, 2.9 \times 10^{-6}]$  and  $[2.5 \times 10^{-7}, 7.8 \times 10^{-7}]$  for  $\theta_{ref} = 0.4, 0.5$  and  $0.6$ , respectively (Fig. 8 shows the results obtained at  $\theta_{ref} = 0.5$ ).

Table 5 shows the parameter values obtained for each river. Although a relatively high correlation could be confirmed for rivers Nos. 3–6 ( $R \geq 0.65$ ), values of  $K$  vary by nearly one order of magnitude. Similarly, the values of  $n$  exhibited inter-river variability;  $n > 1$  for rivers Nos. 3–6, whereas  $n < 1$  for rivers Nos. 1 and 2.

## 5 Discussions

### 5.1 The value of $n$

In Sect. 4.2, the estimated values of  $n$  (1.14 to 1.34) indicate a nonlinear relationship ( $n > 1$ ) between  $E$  and  $k_{sn}$  across  $\theta_{ref}$  of 0.4–0.6. Specifically, for  $\theta_{ref} = 0.5$  and  $0.6$  where  $R \geq 0.5$ , the 90% confidence interval for  $n$  lie entirely above 1.1. This nonlinear relationship is consistent with previous research conducted in various regions, where most estimates of  $n$  are between 1 and 2 (e.g., Ouimet et al., 2009; DiBiase et al., 2010; Lague, 2014; Harel et al., 2016; Campforts et al., 2020; Gallen and Fernandez-Blanco, 2021; Leonard et al., 2023). In addition, slope-break knickpoints occurred at similar elevations across multiple rivers, which do not correspond to boundaries of lithology or different DEM datasets.

Meanwhile, when we compared the averaged  $E$  and  $k_{sn}$  values within detachment-limited reaches,  $n$  was approximately 1 across all  $\theta_{ref}$  values ( $n = 0.96, 0.92$ , and  $0.87$  for  $\theta_{ref} = 0.4, 0.5$ , and  $0.6$ ; Fig. 7d–f). Furthermore, when river No. 1 was excluded and only tributaries within the same drainage area (the Takase River) were compared,  $n$  was 1.05 with a higher  $R$  of 0.79.

To evaluate the robustness of our results, we additionally compared the averaged  $E$  and  $k_{sn-\chi}$ . Similar to previous studies (e.g., Scherler et al., 2014; Neely et al., 2017), channel-averaged local  $k_{sn}$  and  $k_{sn-\chi}$  showed strong correlations ( $R^2 = 0.98$ – $0.99$ ; Fig. S9a–c). Compared with channel-averaged local  $k_{sn}$ , the use of  $k_{sn-\chi}$  yielded slightly smaller  $n$  values (0.75–0.83; Fig. S9d–f). This result is consistent with Scherler et al. (2014) and likely reflects the comparatively smoother nature of  $k_{sn-\chi}$ , which reduces the influence of localized transient steepening associated with slope-break knickpoints. Nevertheless, the overall trends remained unchanged regardless of the choice of  $k_{sn}$ : (1) the nonlinear relationship observed for local  $k_{sn}$  ( $n > 1$ ) weakened toward  $n \sim 1$  when channel-averaged  $k_{sn}$  was used, and (2) excluding river No.1 improved the correlation among tributaries within the Takase River basin.

These results suggest that the observed nonlinearity is likely an apparent effect caused by the presence of migrating knickpoints triggered by sea-level change (Pavano, 2025), rather than reflecting the intrinsic physics of river incision

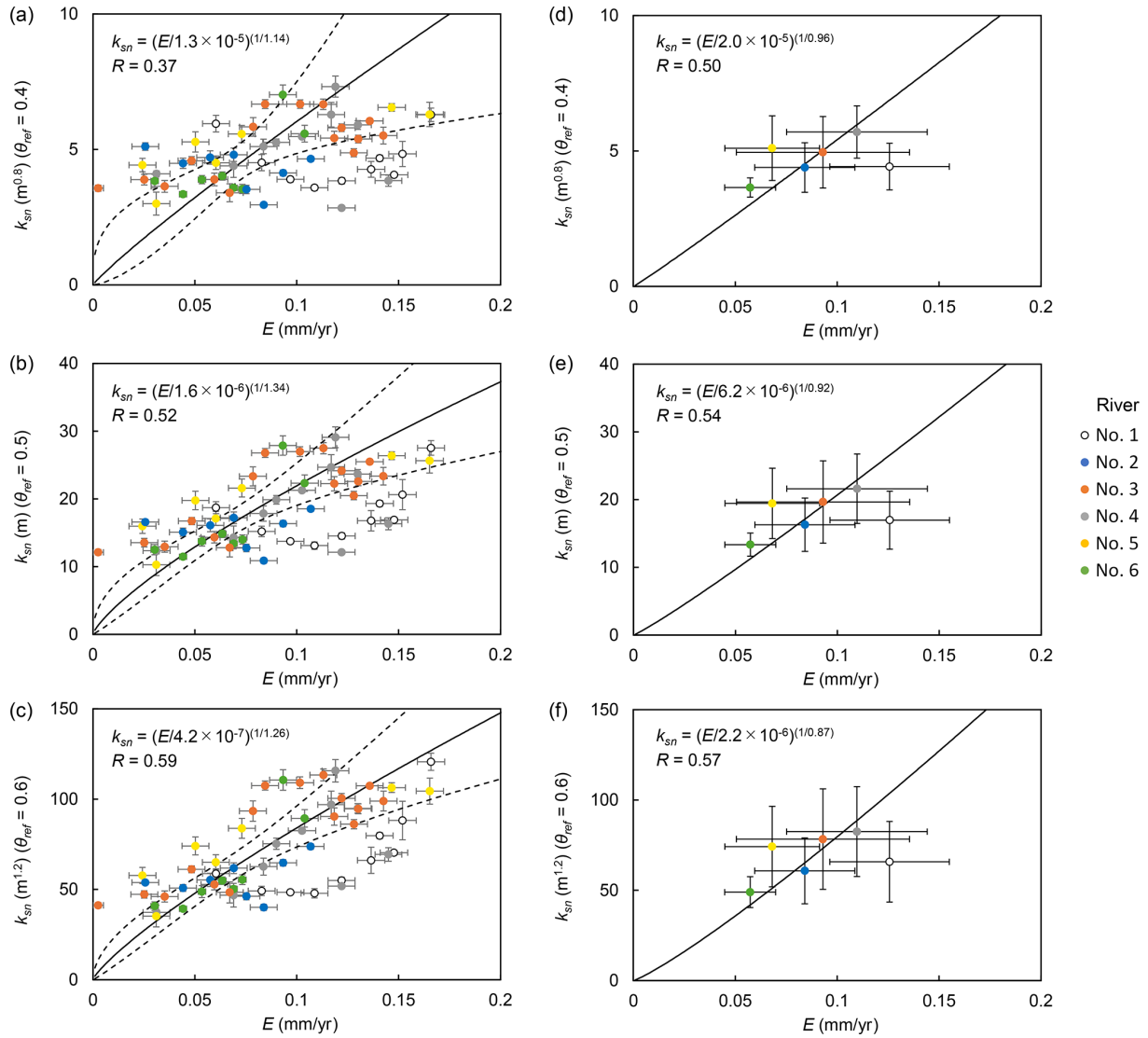


**Figure 7.** River incision rate versus channel steepness index  $k_{sn}$  within the detachment-limited reaches: **(a–c)** sampled at 200 m intervals and **(d–f)** averaged for each reach, both for  $\theta_{ref} = 0.4, 0.5,$  and  $0.6$ . Error bars denote  $\pm 1\sigma$ . The bold and dashed lines indicate the regression lines and their 90 % confidence intervals.

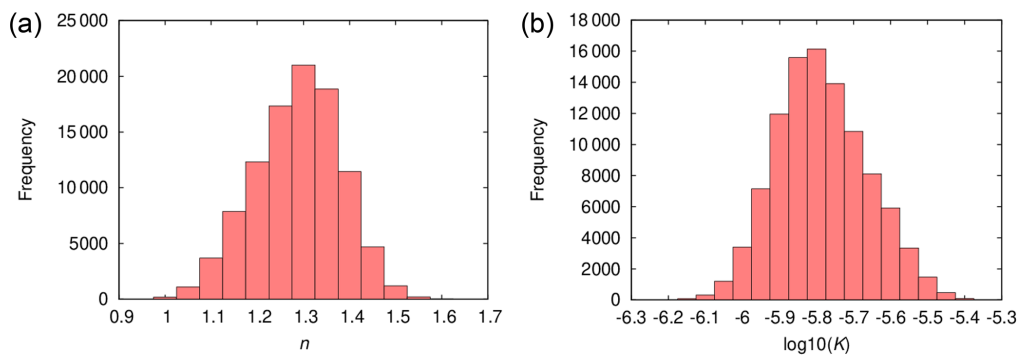


**Figure 8.** Probability distributions of  $n$  and  $K$  values estimated from 100 000 Monte Carlo simulations ( $\theta_{ref} = 0.5$ ).

**Table 5.** River incision parameters ( $n$  and  $K$ ) and correlation coefficient estimated for each river ( $\theta_{\text{ref}}=0.5$ ).

No.	1	2	3	4	5	6
$n$ (–)	0.65	0.72	1.79	1.57	1.36	2.39
$K$	$1.8 \times 10^{-5}$	$9.9 \times 10^{-6}$	$3.6 \times 10^{-7}$	$8.2 \times 10^{-7}$	$1.1 \times 10^{-6}$	$1.1 \times 10^{-7}$
$R$	0.44	0.31	0.57	0.92	0.79	0.66

processes. Although most rivers yield  $n > 1$ , river Nos. 1 or 2 exhibited  $n < 1$ . For river No. 1,  $n < 1$  possibly reflects the differences in watershed and downstream boundary conditions. Unlike other tributaries that flow into the large Lake Ogawara within the Takase River basin (867 km<sup>2</sup>), river No. 1 has a small drainage area (55.9 km<sup>2</sup>) and flows into the small Takahoko pond. These contrasting base-level conditions can lead to different transient response at the catchment scale, causing fluctuations in  $n$  values. For river No. 2, the presence of a lithological boundary, where the downstream lithology is more erodible than upstream lithology, may result in a lower  $n$  value.

Nevertheless, the intrinsic physics of river incision processes may also contribute to the observed nonlinearity. Such physical factors include shear stress thresholds, plucking, channel-width effects, and sediment-flux-dependent incision processes such as abrasion, tool effects, and cover effects (Whipple et al., 2000; Gasparini and Brandon, 2011; Yamanishi and Naruse, 2026). The main target lithology comprises soft sedimentary rocks ( $q_u \leq 3$  MPa, as discussed in Sect. 5.2), where the tool and cover effects of riverbed gravel are likely minimal due to rapid disintegration into fine sediments; however, two possibilities remain: shear stress threshold and abrasion. In the small-scale catchments, the base flow discharge may be insufficient to exceed the critical shear stress required for bedrock incision. In addition, the abundance of sand derived from soft bedrock may cause suspended-load abrasion, which theoretically supports  $n$  values of  $\sim 5/3$  (Whipple et al., 2000). Note that the neglected effect of channel width is limited, since parameter estimation was performed in the limited upstream and midstream areas (Fig. 6). While the relative contributions of these transient responses and physical processes require further comprehensive investigation, the estimated parameters represent robust time-averaged behavior integrated over multi glacial–interglacial cycles.

## 5.2 The value of $K$

The value of  $K$  can vary by orders of magnitude due to lithology, climate, tectonics, hydraulic processes, and other environmental conditions (e.g., Murphy et al., 2016; DiBiase et al., 2018; Chen et al., 2019; Seybold et al., 2021). Among them, Haag and Schoenbohm (2025) confirmed a strong correlation ( $R^2 = 0.89$ ) between global estimates for  $K$  based on <sup>10</sup>Be erosion rates (Harel et al., 2016) and Schmidt hammer-

derived lithologic erodibility ( $K \propto L_E$ ,  $L_E = q_u^{-2}$ ; Sklar and Dietrich, 2001; Turowski et al., 2023); where  $L_E$  is the lithologic erodibility (Campforts et al., 2020) and  $q_u$  is unconfined compressive strength (Fig. 9).

In this section, estimates for  $K$  for this study and the relationship between  $K$  and  $q_u$  in Haag and Schoenbohm (2025) were compared at the same  $\theta_{\text{ref}}$  of 0.5. In the study area, measured  $N$ -values from previous studies for each lithology are as follows (Onuma, 1972; Planning Bureau, Ministry of Construction, Japan, 1997): 25–41 for the terrace deposits, 50–63 for the Hamada and Katchi formations, and 80–137 for the Takahoko formation. We then converted the  $N$ -values to  $q_u$  ( $q_u = 25\text{--}50$  N MPa: Japanese Geotechnical Society, 2015): 0.6–2.0 MPa for the terrace deposits, 1.2–3.1 MPa for the Hamada and Katchi formations, and 2.0–6.8 MPa for the Takahoko formation. For the Hamada and Katchi formations of which the studied rivers mainly consist, estimated values are almost within the 90% confidence interval of the regression line of Haag and Schoenbohm (2025) (Fig. 9). In Sect. 4.2, the estimated  $K$  value was  $1.6 \times 10^{-6}$  [ $1.1 \times 10^{-6}$ ,  $2.9 \times 10^{-6}$ ]. Although rock strength in this study is out of range of the previous study ( $q_u = 10\text{--}100$  MPa), a strong correlation was observed between the results of this study and the data in Haag and Schoenbohm (2025) with  $R^2 = 0.84$ . This highlights the significant influence of bedrock lithology on  $K$ , as indicated by previous research (e.g., Campforts et al., 2020; Haag and Schoenbohm, 2025).

However, the results of this study underestimate  $K$  (the regression line) in the work of Haag and Schoenbohm (2025). This discrepancy is likely caused by three potential reasons. First, as discussed in Sect. 5.1, the influence of sea-level changes may lead to an underestimation of  $K$ . When comparing the average  $k_{sn}$  and  $E$  in the river section, which effectively smooths the transient knickpoint migration due to sea-level changes, the estimated  $K$  value increased to  $6.2 \times 10^{-6}$  [ $7.7 \times 10^{-8}$ ,  $5.1 \times 10^{-4}$ ], approaching the relationship described by Haag and Schoenbohm (2025) (Fig. 9). Note that the estimated  $K$  value using  $k_{sn-\chi}$  remains within the same order of magnitude as that estimated using channel-averaged local  $k_{sn}$ , differing by less than a factor of two (Fig. S9d–f).

Second, the discrepancy may arise from the use of present values of  $k_{sn}$  to compare with long-term average erosion rates. Since the target rivers have been formed gradually by incising the flat marine terraces, long-term average  $k_{sn}$  should be less than the present value. If the long-term aver-

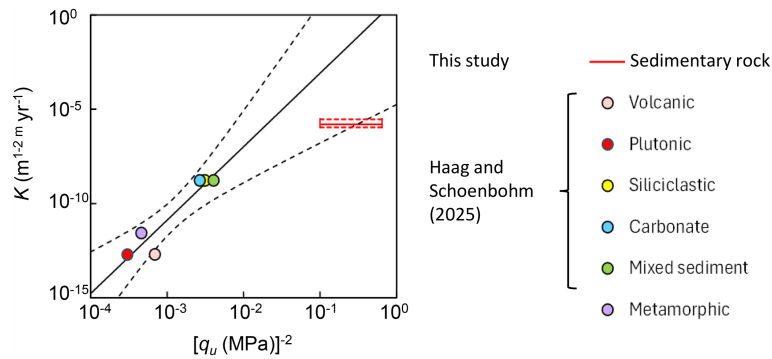


**Figure 9.** Comparison between the results of this study and data of Haag and Schoenbohm (2025) (color points) for unconfined compressive strength  $q_u$  and erosional coefficient  $K$ . The box plot shows the best estimate and 90 % confidence interval of our results based on the log-bin averaged data for all the rivers. The black line and dashed lines are the best estimate and 90 % confidence interval shown in Haag and Schoenbohm (2025).

age  $k_{sn}$  is half of present  $k_{sn}$ , the estimated  $K$  doubles without changing the  $n$  value.

Third, the cohesion of the main riverbed lithologies (the Hamada and Katchi Formations), which are semi-consolidated sedimentary rocks with  $q_u = 1.2\text{--}3.1$  MPa that primarily consist of sandstone and siltstone (see Sect. 2), may function as a resistive factor. This cohesion increases the shear stress threshold and leads to the dissipation of stream power. Since standard mechanical indicators such as  $N$ -values often fail to fully capture the cohesive resistance inherent in these semi-consolidated units, the resulting  $K$  values may fall near the lower bound of the global relationship.

## 6 Conclusions

This study estimated the river incision parameters for soft sedimentary rock, which are lacking in previous global compilations. The study targeted the Kamikita Coastal Plain, where bedrock lithology (sedimentary rocks of Miocene to Pleistocene) and uplift rate (approximately  $0.2\text{ mm yr}^{-1}$  over the past 300 ka) are assumed to be uniform. Parameter values were estimated using slope-area analysis based on river incision rates approximately derived from marine terraces (MIS 5e, 7, 9, and 11) widely distributed in the area. A summary of the main results is as follows.

DL-like behaviour was confirmed in the limited upstream and midstream area ( $A \geq 10^5\text{ m}^2$ ) located upstream of the alluvium distribution for all rivers. Although the optimal  $\theta$  value varied from 0.18 to 0.59 for each river,  $\theta_{\text{ref}}$  was estimated to be  $0.44 \pm 0.10$ , which falls within the typical range for steady-state channels (0.35–0.6).

Across the  $\theta_{\text{ref}}$  range of 0.4 to 0.6, exponent  $n$  consistently exhibited a nonlinear relationship, ranging between 1.14 and 1.34, which aligns with the previous global compilation of 1 to 2. This nonlinearity can be due to past sea-level changes, causing slope-break knickpoints at similar elevations.

For target rivers consisting mainly of late Pliocene and early Pleistocene sedimentary rock, erosion coefficient  $K$  was estimated to be  $10^{-5}\text{--}10^{-6}\text{ m}^{0.1}\text{ yr}^{-1}$ . Estimated  $K$  is almost within 90 % confidence interval of the previous global relationship with unconfined compressive strength  $q_u$  ( $K \propto 1/q_u^2$ ). This supports the significance of bedrock lithology on  $K$ , as previously reported (e.g., Campforts et al., 2020; Haag and Schoenbohm, 2025).

These results represent long-term average erosion trends integrated over multiple glacial–interglacial cycles (since MIS 9 or 11). Consequently, the estimated  $n$  and  $K$  values are considered to reflect integrated values that account for past temporal variations in external forcing, such as climate and sea-level changes. For long-term safety assessments, such as those required for radioactive waste disposal, these parameters serve as a basis for time-dependent simulations of future landscape evolution over a glacial–interglacial cycle ( $\sim 10^4$  to  $10^5$  years). Such simulations can be implemented using mixed DL and TL models, incorporating these time-varying external forcing and additional geomorphic processes, such as hillslope and coastal sediment transport (e.g., Salles et al., 2018). Using the estimated  $n$  and  $K$  values as the baseline, this approach could enable the reliable prediction of not only the maximum erosion depth, but also the spatial distribution of erosion across the site and its subsequent effects on groundwater flow systems. To further verify the estimated parameters, our next step will be the reproduction of past landscape evolution by numerical landscape evolution models using mixed DL and TL models.

**Data availability.** The DEM data is available at Geospatial Information Authority of Japan (<https://service.gsi.go.jp/kiban/>, last access: 27 May 2026). The geological data is available at National Institute of Advanced Industrial Science and Technology (<https://gbank.gsj.jp/seamless/>, last access: 27 May 2026).

**Supplement.** The supplement related to this article is available online at <https://doi.org/10.5194/esurf-14-417-2026-supplement>.

**Author contributions.** S. Takai and T. Sanga designed research. S. Takai and T. Sanga performed research and analyzed data. S. Takai wrote the original manuscript draft and led editing. All authors reviewed and revised the manuscript and approved the final version.

**Competing interests.** The contact author has declared that none of the authors has any competing interests.

**Disclaimer.** Publisher's note: Copernicus Publications remains neutral with regard to jurisdictional claims made in the text, published maps, institutional affiliations, or any other geographical representation in this paper. The authors bear the ultimate responsibility for providing appropriate place names. Views expressed in the text are those of the authors and do not necessarily reflect the views of the publisher.

**Acknowledgements.** The authors would like to thank Prof. T. Sugai of the University of Tokyo, Japan, for his valuable comments. This study was funded by the Secretariat of Nuclear Regulation Authority, Nuclear Regulation Authority, Japan. Sincerely thanks are extended to the one anonymous reviewer and Prof. C. Petit of the Université Côte d'Azur for their essential and constructive comments and suggestions that improved the clarity of this manuscript.

**Review statement.** This paper was edited by Simon Mudd and reviewed by Carole Petit and one anonymous referee.

## References

- Adams, B. A., Whipple, K. X., Forte, A. M., Heimsath, M., and Hodges, K.V.: Climate controls on erosion in tectonically active landscapes, *Sci. Adv.*, 6, eaaz3166, <https://doi.org/10.1126/sciadv.aaz3166>, 2020.
- AIST (National Institute of Advanced Industrial Science and Technology): The 2016 fiscal year project report of expenses for commission of safety review for geological disposal of radioactive waste: Evaluation methods toward safety review – geological information section, <https://www.nsr.go.jp/data/000192112.pdf> (last access: 5 December 2025), 2015 (in Japanese).
- AIST (National Institute of Advanced Industrial Science and Technology): The 2017 fiscal year project report of expenses for commission of safety control for nuclear power plant facilities: Reconnaissance investigation for long-term prediction of natural disaster, <https://www.nsr.go.jp/data/000186554.pdf> (last access: 5 December 2025), 2016 (in Japanese).
- AIST (National Institute of Advanced Industrial Science and Technology): Seamless digital geological map of Japan V2 1 : 200 000, Original edition, <https://gbank.gsj.jp/seamless/> (last access: 5 December 2025), 2025.
- Alcalde, J., Flude, S., Wilkinson, M., Johnson, G., Edlmann, K., Bond, C. E., Scott, V., Gilfillan, S. M. V., Ogaya, X., and Haszeldine, R. S.: Estimating geological CO<sub>2</sub> storage security to deliver on climate mitigation, *Nat. Commun.*, 9, 2201, <https://doi.org/10.1038/s41467-018-04423-1>, 2018.
- Armitage, J. J., Whittaker, A. C., Zakari, M., and Campforts, B.: Numerical modelling of landscape and sediment flux response to precipitation rate change, *Earth Surf. Dynam.*, 6, 77–99, <https://doi.org/10.5194/esurf-6-77-2018>, 2018.
- Bishop, P., Hoey, T. B., Jansen, J. D., and Artza, I. L.: Knick-point recession rate and catchment area: the case of uplifted rivers in Eastern Scotland, *Earth Surf. Proc. Land.*, 778, 767–778, <https://doi.org/10.1002/esp.1191>, 2005.
- Boulton, S. J.: Geomorphic response to differential uplift: River long profiles and knickpoints from Guadalcanal and Makira (Solomon Islands), *Front. Earth Sci.*, 8, 10, <https://doi.org/10.3389/feart.2020.00010>, 2020.
- Campforts, B. and Govers, G.: Keeping the edge: A numerical method that avoids knickpoint smearing when solving the stream power law, *J. Geophys. Res.-Earth*, 120, 1189–1205, <https://doi.org/10.1002/2014JF003376>, 2015.
- Campforts, B., Vanacker, V., Herman, F., Vanmaercke, M., Schwanghart, W., Tenorio, G. E., Willems, P., and Govers, G.: Parameterization of river incision models requires accounting for environmental heterogeneity: insights from the tropical Andes, *Earth Surf. Dynam.*, 8, 447–470, <https://doi.org/10.5194/esurf-8-447-2020>, 2020.
- Chen, S. A., Michaelides, K., Grieve, S. W. D., and Singer, M. B.: Aridity is expressed in river topography globally, *Nature*, 573, 573–577, <https://doi.org/10.1038/s41586-019-1558-8>, 2019.
- Desormeaux, C., Godard, V., Lague, D., Duclaux, G., Fleury, J., Benedetti, L., Bellier, O., and the ASTER Team: Investigation of stochastic-threshold incision models across a climatic and morphological gradient, *Earth Surf. Dynam.*, 10, 473–492, <https://doi.org/10.5194/esurf-10-473-2022>, 2022.
- DiBiase, R. A., Whipple, K. X., Heimsath, A. M., and Ouimet, W. B.: Landscape form and millennial erosion rates in the San Gabriel Mountains, CA, *Earth Planet. Sc. Lett.*, 289, 134–144, <https://doi.org/10.1016/j.epsl.2009.10.036>, 2010.
- DiBiase, R. A., Rossi, M. W., and Neely, A. B.: Fracture density and grain size controls on the relief structure of bedrock landscapes, *Geology*, 46, 399–402, <https://doi.org/10.1130/G40006.1>, 2018.
- Duvall, A., Kirby, E., and Burbank, D.: Tectonic and lithologic controls on bedrock channel profiles and processes in coastal California, *J. Geophys. Res.*, 109, F03002, <https://doi.org/10.1029/2003JF000086>, 2004.
- Flint, J. J.: Stream gradient as a function of order, magnitude, and discharge, *Water Resour. Res.*, 10, 969–973, <https://doi.org/10.1029/WR010i005p00969>, 1974.
- Gaillaton, B., Mudd, S. M., Clubb, F. J., Peifer, D., and Hurst, M. D.: A segmentation approach for the reproducible extraction and quantification of knickpoints from river long profiles, *Earth Surf. Dynam.*, 7, 211–230, <https://doi.org/10.5194/esurf-7-211-2019>, 2019.
- Gallen, S. F. and Fernandez-Blanco, D.: A new data-driven Bayesian inversion of fluvial topography clarifies the tectonic history of the Corinth Rift and reveals a channel steepness threshold, *J. Geophys. Res.-Earth*, 126, <https://doi.org/10.1029/2020JF005651>, 2021.

- Gasparini, N. M. and Brandon, M. T.: A generalized power law approximation for fluvial incision of bedrock channels, *J. Geophys. Res.*, 116, <https://doi.org/10.1029/2009jf001655>, 2011.
- Gesch, D. B.: The national elevation dataset, in: *Digital Elevation Model Technologies and Applications: The DEM Users Manual*, 2nd edn., edited by: Manue, D., American Society for Photogrammetry and Remote Sensing, Bethesda, Maryland, 99–118, ISBN: 978-1-570-83082-2, 2007.
- GIA (Geospatial Information Authority of Japan): Methods for creating elevation tiles and elevation values displayed on GSI Maps, <https://maps.gsi.go.jp/development/hyokochi.html> (last access: 15 April 2026), 2026 (in Japanese).
- Haag, M. B. and Schoenbohm, L. M.: Thor: a rock strength database for investigating lithologic controls in landscape evolution, *Earth Planet. Sc. Lett.*, 660, <https://doi.org/10.1016/j.epsl.2025.119364>, 2025.
- Hack, J. T.: Studies of longitudinal stream profiles in Virginia and Maryland, U.S. Geol. Surv. Prof. Pap., 294–B, <https://pubs.usgs.gov/pp/0294b/report.pdf> (last access: 27 May 2026), 1957.
- Harel, M. A., Mudd, S. M., and Attal, M.: Global analysis of the stream power law parameters based on worldwide  $^{10}\text{Be}$  denudation rates, *Geomorphology*, 268, 184–196, <https://doi.org/10.1016/j.geomorph.2016.05.035>, 2016.
- Haviv, I., Enzel, Y., Whipple, K. X., Zilberman, E., Matmon, A., Stone, J., and Fifield, K., L.: Evolution of vertical knickpoints (waterfalls) with resistant caprock: Insights from numerical modeling, *J. Geophys. Res.-Earth*, 115, <https://doi.org/10.1029/2008JF001187>, 2010.
- Henderson, F.: *Open Channel Flow*, MacMillan, New York, 522 pp., ISBN 9780023535109, 1966.
- Hergarten, S.: Transport-limited fluvial erosion – simple formulation and efficient numerical treatment, *Earth Surf. Dynam.*, 8, 841–854, <https://doi.org/10.5194/esurf-8-841-2020>, 2020.
- Hilley, G. E., Porder, S., Aron, F., Baden, C. W., Johnstone, S. A., Liu, F., Sare, R., Steelquist, A., and Young, H. H.: Earth's topographic relief potentially limited by an upper bound on channel steepness, *Nat. Geosci.*, 12, 828–832, <https://doi.org/10.1038/s41561-019-0442-3>, 2019.
- Howard, A. D.: A detachment-limited model of drainage basin evolution, *Water Resour. Res.*, 30, 2261–2285, <https://doi.org/10.1029/94WR00757>, 1994.
- Howard, A. D. and Kerby, G.: Channel changes in badlands, *Geol. Soc. Am. Bull.*, 94, 739–752, [https://doi.org/10.1130/0016-7606\(1983\)94<739:CCIB>2.0.CO;2](https://doi.org/10.1130/0016-7606(1983)94<739:CCIB>2.0.CO;2), 1983.
- Hu, X., Zhang, Y., Guo, J., and Pan, B.: How does climate affect the topography in tectonically active orogens, *Earth Surf. Proc. Land.*, 48, 1267–1280, <https://doi.org/10.1002/esp.5547>, 2023.
- Inohara, Y., Oyama, T., and Torigoe, Y.: Magnetic Susceptibility Analysis of Takahoko Formation at Simokita Peninsula, Northeast Japan, *J. Jpn. Soc. Eng. Geol.*, 49, 3, 139–149, <https://doi.org/10.5110/jjseg.49.139>, 2008 (in Japanese with English summary).
- IPCC: IPCC special report on carbon dioxide capture and storage, prepared by Working Group III of the Intergovernmental Panel on Climate Change, edited by: Metz, B., Davidson, O., de Coninck, H. C., Loos, M., and Meyer, L., Cambridge University Press, Cambridge, United Kingdom and New York, NY, USA, 431 pp., ISBN: 978-0-521-68551-1, 2005.
- Japanese Geotechnical Society: Japan geotechnical society standard – Geotechnical and geoenvironmental investigation methods, Vol. 1, ISBN 9784886448231, 2015.
- Japan Meteorological Agency (JMA): Past weather data search, <https://www.data.jma.go.jp/stats/etrm/index.php>, last access: 19 January 2026 (in Japanese).
- Kirby, E. and Whipple, K. X.: Quantifying differential rock-uplift rates via stream profile analysis, *Geology*, 29, 415–418, [https://doi.org/10.1130/0091-7613\(2001\)029<0415:QDRURV>2.0.CO;2](https://doi.org/10.1130/0091-7613(2001)029<0415:QDRURV>2.0.CO;2), 2001.
- Kirby, E. and Whipple, K. X.: Expression of active tectonics in erosional landscapes, *J. Struct. Geol.*, 44, 54–75, <https://doi.org/10.1016/j.jsg.2012.07.009>, 2012.
- Koike, K. and Machida, H.: *Atlas of Quaternary Marine Terraces in the Japanese Islands*, University of Tokyo Press, Tokyo, 105 pp., ISBN: 4-13-060735-9, 2001.
- Kudo, T., Horiuchi, S., and Yanagisawa, Y.: Chronostratigraphy of the Lower to Middle Miocene in the eastern part of Shimokita Peninsula, Northeast Japan, *Bull. Geol. Surv. Japan*, 71, 5, 439–462, 2020 (in Japanese with English summary).
- Kudo, T.: Cumulative volume step-diagram for eruptive magmas of Towada Volcano, *Bull. Geol. Surv. Japan*, 74, 3, 133–153, 2023 (in Japanese with English summary).
- Kuwabara, T.: Relative sea-level changes and marine-terrace deposits in Kamikita plain, northern end of Honshu, Japan, *J. Geol. Soc. Japan*, 110, 93–102, <https://doi.org/10.5575/geosoc.110.93>, 2004 (in Japanese with English summary).
- Kuwabara, T.: Fission-track dating of the middle-pleistocene shiro-beta tephra (WP) in the Kamikita Plain, northeast Japan, *Quat. Res. Jpn.*, 46, 433–436, <https://doi.org/10.4116/jaqua.46.433>, 2007 (in Japanese).
- Kuwabara, T.: Environmental change and its correlation to terraces based on phytolith assemblage of tephra-soil succession after the later half of the middle Pleistocene drilled on the Kamikita Plain, NE Japan, *Quat. Res. Jpn.*, 48, 405–416, <https://doi.org/10.4116/jaqua.48.405>, 2009 (in Japanese with English summary).
- Lague, D.: The stream power river incision mode: evidence, theory and beyond, *Earth Surf. Proc. Land.*, 39, 38–61, <https://doi.org/10.1002/esp.3462>, 2014.
- Lal, D.: Cosmic ray labeling of erosion surfaces: in situ nuclide production rates and erosion models, *Earth Planet. Sci. Lett.*, 104, 424–439, [https://doi.org/10.1016/0012-821X\(91\)90220-C](https://doi.org/10.1016/0012-821X(91)90220-C), 1991.
- Leonard, J. S., Whipple, K. X., and Heimsath, A. M.: Controls on topography and erosion of the north-central Andes, *Geology*, 52, 153–158, <https://doi.org/10.1130/G51618.1>, 2023.
- Liu, Z., Han, L., Boulton, S. J., Wu, T., and Guo, J.: Quantifying the transient landscape response to active faulting using fluvial geomorphic analysis in the Qianhe Graben on the southwest margin of Ordos, China, *Geomorphology*, 351, 106974, <https://doi.org/10.1016/j.geomorph.2019.106974>, 2020.
- Marder, E. and Gallen S. F.: Climate control on the relationship between erosion rate and fluvial topography, *Geology*, 51, 5, 424–427, <https://doi.org/10.1130/G50832.1>, 2023.
- Matsu'ura, T., Komatsubara, J., and Wu, C.: Accurate determination of the Pleistocene uplift rate of the NE Japan forearc from the buried MIS 5e marine terrace shoreline angle, *Quat. Sci. Rev.*,

- 212, 45–68, <https://doi.org/10.1016/j.quascirev.2019.03.007>, 2019.
- Miyauchi, T.: Quaternary crustal movements estimated from deformed terraces and geologic structures of the Kamikita coastal plain, northeast Japan, *Geogr. Rev. Jpn.*, 58, 492–515, [https://doi.org/10.4157/grj1984a.58.8\\_492](https://doi.org/10.4157/grj1984a.58.8_492), 1985 (in Japanese with English summary).
- MLIT (Ministry of Land, Infrastructure, Transport and Tourism of Japan): River improvement plan of Takase River, <https://www.thr.mlit.go.jp/takase/committe/keikaku/pdf/keikaku.pdf> (last access: 13 April 2026), 2006 (in Japanese).
- Montgomery, D. R. and Foufoula-Georgiou, E.: Channel network source representation using digital elevation models, *Water Resour. Res.*, 29, 3925–3934, <https://doi.org/10.1029/93WR02463>, 1993.
- Morisawa, M. E.: Quantitative geomorphology of some watersheds in the Appalachian Plateau, *Geol. Soc. Am. Bull.*, 73, 1025–1046, [https://doi.org/10.1130/0016-7606\(1962\)73\[1025:QGOSWI\]2.0.CO;2](https://doi.org/10.1130/0016-7606(1962)73[1025:QGOSWI]2.0.CO;2), 1962.
- Mudd, S. M., Attal, M., Milodowski, D. T., Grieve, S. W., and Valters, D. A.: A statistical framework to quantify spatial variation in channel gradients using the integral method of channel profile analysis, *J. Geophys. Res.-Earth*, 119, 138–152, <https://doi.org/10.1002/2013JF002981>, 2014.
- Murphy, B. P., Johnson, J. P. L., Gasparini, N. M., and Sklar L. S.: Chemical weathering as a mechanism for the climatic control of bedrock river incision, *Nature*, 532, 223–227, <https://doi.org/10.1038/nature17449>, 2016.
- Neely, A. B., Bookhagen, B., and Burbank, D. W.: An automated knickzone selection algorithm (KZ-Picker) to analyze transient landscapes: Calibration and validation, *J. Geophys. Res.-Earth Surf.*, 122, 1236–1261, <https://doi.org/10.1002/2017JF004250>, 2017.
- Nemoto, N. and Ujiie, Y.: Geology of Aomori prefecture, in: Daichi, Tohoku Geotechnical Consultants Association, Miyagi, Japan, 52–68, <https://tohoku-geo.ne.jp/information/daichi/img/50a/52.pdf> (last access: 17 April 2026), 2009 (in Japanese).
- NRA (Nuclear Regulation Authority): Interpretation of the location, structure and equipment for Category 2 waste disposal facilities (enacted on 27 November 2013, revised on 13 November 2019 and 29 September 2021), <https://www.nra.go.jp/data/000069192.pdf> (last access: 22 April 2026), 2021 (in Japanese).
- NUMO (Nuclear Waste Management Organization of Japan): The NUMO Pre-siting SDM-based Safety Case, NUMO-TR-21-01, [https://www.numo.or.jp/technology/technical\\_report/pdf/NUMO-TR21-01\\_rev260127.pdf](https://www.numo.or.jp/technology/technical_report/pdf/NUMO-TR21-01_rev260127.pdf) (last access: 27 May 2026), 2021.
- Ogami, T.: Dynamics of longitudinal river profiles associated with knickpoints since the Middle Pleistocene on the northern Sanriku Coast, NE Japan, *The Quaternary Research (Daiyonki-Kenkyu)*, 54, 113–128, <https://doi.org/10.4116/jaqua.54.113>, 2015 (in Japanese with English summary).
- Onuma, Z.: Geological character of Mutsu-Ogawara area Aomori prefecture, *Jour. Japan Soc. Eng. Geol.*, 13, 8–22, <https://doi.org/10.5110/jjseg.13.8>, 1972 (in Japanese with English summary).
- Ott, R. F., Perez-Consuegra, N., Scherler, D., Mora, A., Huppert, K. L., Braun, J., Hoke, G. D., and Sandoval Ruiz, J. R.: Erosion rate maps highlight spatio-temporal patterns of uplift and quantify sediment export of the Northern Andes, *Earth Planet. Sc. Lett.*, 621, 118354, <https://doi.org/10.1016/j.epsl.2023.118354>, 2023.
- Ouimet, W. B., Whipple, K. X., and Granger, D. E.: Beyond threshold hillslopes: Channel adjustment to base-level fall in tectonically active mountain ranges, *Geology*, 37, 579–582, <https://doi.org/10.1130/G30013A.1>, 2009.
- Pavano, F.: Fault geometry, strain partitioning and deformation history inferred by fluvial topography and marine terrace analyses, *Geomorphology*, 472, <https://doi.org/10.1016/j.geomorph.2024.109583>, 2025.
- Perron, J. T. and Royden, L.: An integral approach to bedrock river profile analysis, *Earth Surf. Proc. Land.*, 38, 570–576, <https://doi.org/10.1002/esp.3302>, 2013.
- Planning Bureau, Ministry of Construction, Japan: General description of the ground in the Hachinohe and Misawa areas in Aomori prefecture, 1997 (in Japanese).
- Salles, T., Ding, X., and Brocard, G.: pyBadlands: A framework to simulate sediment transport, landscape dynamics and basin stratigraphic evolution through space and time, *PLoS ONE*, 13, 4, e0195557, <https://doi.org/10.1371/journal.pone.0195557>, 2018.
- Scherler, D., Bookhagen, B., and Strecker, M. R.: Tectonic control on <sup>10</sup>Be-derived erosion rates in the Garhwal Himalaya, India, *J. Geophys. Res.-Earth*, 119, 83–105, <https://doi.org/10.1002/2013JF002955>, 2014.
- Seybold, H., Berghuijs, W. R., Prancevic, J. P., and Kirchner, J. W.: Global dominance of tectonics over climate in shaping river longitudinal profiles, *Nat. Geosci.*, 14, 503–507, <https://doi.org/10.1038/s41561-021-00720-5>, 2021.
- Sklar, L. S. and Dietrich, W. E.: Sediment and rock strength controls on river incision into bedrock, *Geology*, 29, 1087–1090, [https://doi.org/10.1130/0091-7613\(2001\)029<1087:SARSCO>2.0.CO;2](https://doi.org/10.1130/0091-7613(2001)029<1087:SARSCO>2.0.CO;2), 2001.
- Snyder, N. P., Whipple, K. X., Tucker, G. E., and Merritts, D. J.: Landscape response to tectonic forcing: Digital elevation model analysis of stream profiles in the Mendocino triple junction region, northern California, *Geol. Soc. Am. Bull.*, 112, 1250–1263, [https://doi.org/10.1130/0016-7606\(2000\)112<1250:LRTTFD>2.0.CO;2](https://doi.org/10.1130/0016-7606(2000)112<1250:LRTTFD>2.0.CO;2), 2000.
- Snyder, N. P., Whipple, K. X., Tucker, G. E., and Merritts, D. J.: Interactions between onshore bedrock-channel incision and nearshore wave-base erosion forced by eustasy and tectonics, *Basin Res.*, 14, 105–127, <https://doi.org/10.1046/j.1365-2117.2002.00169.x>, 2003.
- SSM (Swedish Radiation Safety Authority): The Swedish Radiation Safety Authority's regulations concerning the protection of human health and the environment in connection with the final management of spent nuclear fuel and nuclear waste, SSMFS 2008:37, <https://www.stralsakerhetsmyndigheten.se/en/publications/regulations/ssmfs-english/ssmfs-200837/> (last access: 27 May 2026), 2008.
- Stock, J. and Dietrich, W. E.: Valley incision by debris flows: Evidence of a topographic signature, *Water Resour. Res.*, 39, <https://doi.org/10.1029/2001WR001057>, 2003.
- Stock, J. D., Montgomery, D. R., Collins, B. D., Dietrich, W. E., and Sklar, L.: Field measurements of incision rates following bedrock exposure: implications for process controls on the long profiles of valleys cut by rivers and debris flows, *Geol. Soc. Am. Bull.*, 117, 174–194, <https://doi.org/10.1130/B25560.1>, 2005.

- Takahashi, N. O., Shyu, J. B. H., Chen, C., and Toda, S.: Long-term uplift pattern recorded by rivers across contrasting lithology: Insights into earthquake recurrence in the epicentral area of the 2016 Kumamoto earthquake, Japan, *Geomorphology*, 419, <https://doi.org/10.1016/j.geomorph.2022.108492>, 2022.
- Takahashi, N. O., Shyu, J. B. H., Toda, S., Matsushi, Y., Ohta, R. J., and Matsuzaki, H.: Transient Response and Adjustment Timescales of Channel Width and Angle of Valley-Side Slopes to Accelerated Incision, *J. Geophys. Res.-Earth*, 128, e2022JF006967, <https://doi.org/10.1029/2022JF006967>, 2023.
- Tarboton, D. G., Bras, R. L., and Rodriguez-Iturbe, I.: On the extraction of channel networks from digital elevation data, *Hydrol. Process.*, 5, 81–100, <https://doi.org/10.1002/hyp.3360050107>, 1991.
- Turowski, J. M., Pruß, G., Voigtländer, A., Ludwig, A., Landgraf, A., Kober, F., and Bonnelye, A.: Geotechnical controls on erodibility in fluvial impact erosion, *Earth Surf. Dynam.*, 11, 979–994, <https://doi.org/10.5194/esurf-11-979-2023>, 2023.
- Vanacker, V., Blanckenburg, F. V., Govers, G., Molina, A., Campforts, B., and Kubik, P. W.: Transient river response, captured by channel steepness and its concavity, *Geomorphology*, 228, 234–243, <https://doi.org/10.1016/j.geomorph.2014.09.013>, 2015.
- von Blanckenburg, F.: The control mechanisms of erosion and weathering at basin scale from cosmogenic nuclides in river sediment, *Earth Planet. Sc. Lett.*, 242, 224–239, <https://doi.org/10.1016/j.epsl.2005.11.017>, 2006.
- Wang, Y., Zhang, H., Zheng, D., Yu, J., Pang, J., and Ma, Y.: Coupling slope–area analysis, integral approach and statistic tests to steady-state bedrock river profile analysis, *Earth Surf. Dynam.*, 5, 145–160, <https://doi.org/10.5194/esurf-5-145-2017>, 2017.
- Whipple, K. X.: Bedrock rivers and the geomorphology of active orogens, *Annu. Rev. Earth. Pl. Sc.*, 32, 151–185, <https://doi.org/10.1146/annurev.earth.32.101802.120356>, 2004.
- Whipple, K. X. and Tucker, G. E.: Dynamics of the stream-power river incision model: Implications for height limits of mountain ranges, landscape response timescales, and research needs, *J. Geophys. Res.*, 104, 17661–17674, <https://doi.org/10.1029/1999JB900120>, 1999.
- Whipple, K. X. and Tucker, G. E.: Implications of sediment-flux-dependent river incision models for landscape evolution, *J. Geophys. Res.*, 107, 2039, <https://doi.org/10.1029/2000JB000044>, 2002.
- Whipple, K. X., Hancock, G. S., and Anderson, R. S.: River incision into bedrock: Mechanics and relative efficacy of plucking, abrasion and cavitation, *GSA Bulletin*, 112, 3, 490–503, [https://doi.org/10.1130/0016-7606\(2000\)112<490:RIIBMA>2.0.CO;2](https://doi.org/10.1130/0016-7606(2000)112<490:RIIBMA>2.0.CO;2), 2000.
- Whipple, K. X., Wobuc, C., Crosby, B., Kirby, E., and Sheehan, D.: New tools for quantitative geomorphology: extraction and interpretation of stream profiles from digital topographic data, *GSA Short Course*, 506, 1–26, 2007.
- Whipple, K. X., DiBiase, R., and Crosby, B.: 9.28 Bedrock Rivers, 9, 550–573, ISBN 9780080885223, <https://doi.org/10.1016/B978-0-12-374739-6.00254-2>, 2013.
- Wobus, C., Whipple, K. X., Kirby, E., Snyder, N., Johnson, J., Spyropoulou, K., Crosby, B., and Sheehan, D.: Tectonics from topography: procedures, promise, and pitfalls, in *Tectonics, Climate, and Landscape Evolution*, Geological Society of America, 398, 55–74, [https://doi.org/10.1130/2006.2398\(04\)](https://doi.org/10.1130/2006.2398(04)), 2006.
- Yamanishi, N. and Naruse, H.: Limited influence of bedrock strength on river profiles: the dominant role of sediment dynamics, *Earth Surf. Dynam.*, 14, 247–268, <https://doi.org/10.5194/esurf-14-247-2026>, 2026.